

Quantized conductance doubling and hard gap in a two-dimensional semiconductor-superconductor heterostructure

M. Kjaergaard,¹ F. Nichele,¹ H. J. Suominen,¹ M. P. Nowak,^{2,3,4} M. Wimmer,^{2,3} A. R. Akhmerov,² J. A. Folk,^{5,6} K. Flensberg,¹ J. Shabani,^{7,*} C. J. Palmström,⁷ and C. M. Marcus¹

¹*Center for Quantum Devices and Station Q Copenhagen, Niels Bohr Institute, University of Copenhagen, Universitetsparken 5, 2100 Copenhagen, Denmark*

²*Kavli Institute of Nanoscience, Delft University of Technology, P.O. Box 4056, 2600 GA Delft, The Netherlands*

³*QuTech, Delft University of Technology, P.O. Box 4056, 2600 GA Delft, The Netherlands*

⁴*AGH University of Science and Technology, Faculty of Physics and Applied Computer Science, al. Mickiewicza 30, 30-059 Kraków, Poland*

⁵*Department of Physics and Astronomy, University of British Columbia, Vancouver, British Columbia, V6T1Z1, Canada*

⁶*Quantum Matter Institute, University of British Columbia, Vancouver, BC, V6T1Z4, Canada*

⁷*California NanoSystems Institute, University of California, Santa Barbara, CA 93106, USA*

(Dated: March 26, 2022)

The prospect of coupling a two-dimensional (2D) semiconductor heterostructure to a superconductor opens new research and technology opportunities, including fundamental problems in mesoscopic superconductivity [1–3], scalable superconducting electronics [4, 5], and new topological states of matter [6]. For instance, one route toward realizing topological matter is by coupling a 2D electron gas (2DEG) with strong spin-orbit interaction to an s-wave superconductor [6–8]. Previous efforts along these lines have been hindered by interface disorder and unstable gating [9–11]. Here, we report measurements on a gateable InGaAs/InAs 2DEG with patterned epitaxial Al, yielding multilayer devices with atomically pristine interfaces between semiconductor and superconductor [12]. Using surface gates to form a quantum point contact (QPC), we find a hard superconducting gap in the tunneling regime, overcoming the soft-gap problem in 2D superconductor/semiconductor hybrid systems [13]. With the QPC in the open regime, we observe a first conductance plateau at $4e^2/h$, as expected theoretically for a normal-QPC-superconductor structure [14]. The realization of a hard-gap semiconductor-superconductor system that is amenable to top-down processing provides a means of fabricating scalable multicomponent hybrid systems for applications in low-dissipation electronics and topological quantum information.

Recent work on semiconductor nanowires has offered evidence for the existence of Majorana zero modes, a signature of the topological superconductivity [15–17]. A characteristic of the first studies in this area was significant subgap tunneling conductance (a so-called soft gap), attributed to disorder at the semiconductor-superconductor (Sm-S) interface along with dissipation

[13, 18]. In nanowires, the soft-gap problem was recently resolved by growing Al epitaxially on InAs nanowires, yielding greatly reduced subgap conductance [19, 20]. Studies of Sm-S systems based on top-down processed 2DEGs have not addressed the soft-gap issue, but have demonstrated quantization of critical current [21, 22], retro-reflection by Andreev scattering [23], and spectroscopy of a gate-defined quantum dot with superconducting leads [24, 25], which do not require a hard proximity-induced gap in the semiconductor.

The two main results presented here are both consequences of the transparent epitaxial Sm-S interface. The first is a doubling of the the lowest quantized conductance plateau, from $2e^2/h$ in the normal state to $4e^2/h$ in the superconducting state, as predicted theoretically [14]. The second is a strong suppression of conductance for voltages smaller than the superconducting gap when

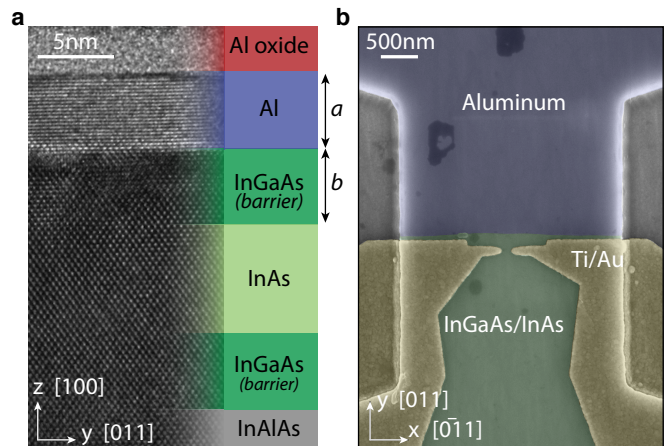


FIG. 1: **Epitaxial aluminium on InGaAs/InAs and device layout.** **a**, Cross-sectional transmission electron micrograph of epitaxial Al on InGaAs/InAs. On the wafer imaged here, the height of the InGaAs barrier is $b = 5$ nm and Al film thickness $a \sim 5$ nm. **b**, False-color scanning electron micrograph of Device 1 (see main text for details).

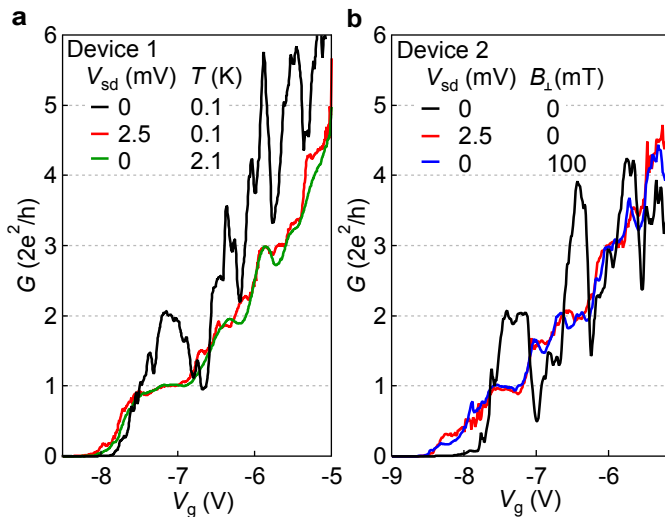


FIG. 2: **Quantized conductance in the Andreev quantum point contact.** **a**, Differential conductance, G , as a function of gate voltage V_g at zero bias (black line), at source-drain bias larger than the gap (red line), and at elevated temperature (green line). At zero bias and base temperature, the first conductance plateau is at $4e^2/h$, double the value at higher temperature or bias. **b**, The differential conductance in a second, lithographically identical, device at zero bias (black line), at source-drain bias larger than the gap (red line), and in a magnetic field applied perpendicular to the plane of the chip (blue line).

the QPC is in the tunneling regime—that is, the detection of a hard superconducting gap in a proximitized 2DEG. Conductance doubling arises from Andreev reflection transferring charge $2e$ into the superconductor [26]. The hard gap reflects the absence of electronic states below the superconducting gap in the semiconductor. Using gate voltage to control the QPC, we measure conductance across the transition from weak tunneling to the open-channel regime and find good (but not perfect) agreement with the theory of a normal-QPC-superconductor structure [14].

The starting material is an undoped InAs/InGaAs heterostructure with epitaxial Al as a top layer, grown by molecular beam epitaxy [12]. A cross-sectional TEM showing a sharp epitaxial Sm-S interface is shown in Fig. 1a. In the devices reported here, the thickness of the InGaAs barrier was $b = 10$ nm, and the Al film was $a = 10$ nm. A Hall ball fabricated on the same wafer with the Al removed (using Transene D aluminum etch) gave density $n = 3 \cdot 10^{12} \text{ cm}^{-2}$ and mobility $\mu = 10^4 \text{ cm}^2/\text{Vs}$, yielding a mean free path $l_e \sim 230$ nm. In a similar wafer, weak anti-localization analysis gave a spin-orbit length $l_{so} \sim 45$ nm [12]. The Al film has a critical temperature $T_c = 1.56$ K, corresponding to a gap $\Delta_0 = 235 \mu\text{eV}$, enhanced from the bulk value of Al, and consistent with other measurements on Al films of similar thickness [27]. The in-plane critical field of the Al film is $B_c = 1.65$ T [12]. Ohmic contacts to the InAs electron gas are formed by the epitaxial Al directly and mesa

structures are patterned by standard III-V chemical etching techniques. An insulating 40 nm Al_2O_3 layer is deposited using atomic layer deposition and metallic gates (5 nm Ti/50 nm Au) are evaporated onto the device. The measurements were performed in a dilution refrigerator with a base mixing chamber temperature $T_{\text{mc}} \sim 30$ mK, using four-terminal lock-in techniques and DC measurements. Two lithographically similar devices were measured, with similar results.

A scanning electron micrograph of Device 1 is shown in Fig. 1b. The conductance of the QPC is tuned by negative voltages applied to the gates. The QPC is located ~ 150 nm in front of the region where the Al film has not been removed. Figure 2 shows conductance traces for the two lithographically similar QPCs. In the superconducting state, both devices show increased conductance at the plateau of the QPC and suppressed conductance below $G \sim 0.8G_0$, where $G_0 \equiv 2e^2/h$, relative to the normal state. This behavior is the hallmark of Andreev reflection being the dominant conduction mechanism through the QPC [14, 28]. Raising the temperature above the critical temperature of the Al film, applying an out-of-plane magnetic field, or applying a bias larger than the gap, all bring the lowest plateau back to $2e^2/h$ (see Fig. 2). The dip structure, observed in both samples, at the transition between conductance plateaus could be caused by mode

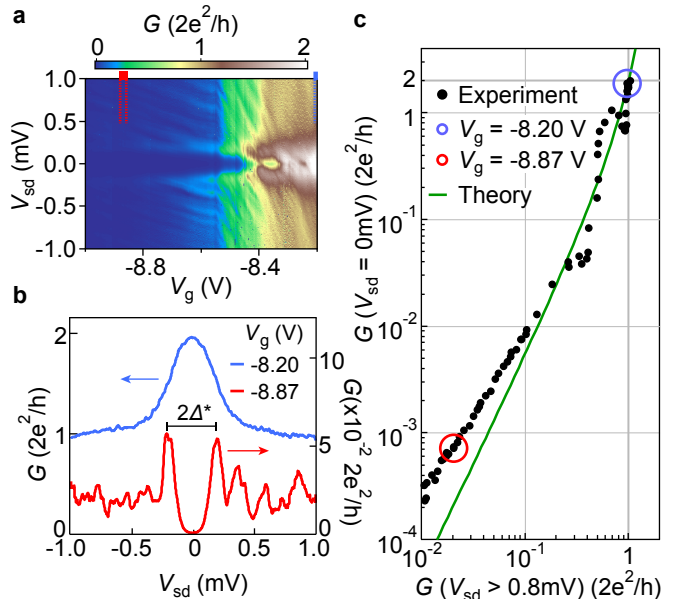


FIG. 3: **Transition from $4e^2/h$ conductance to hard superconducting gap.** **a**, Differential conductance, G , in Device 1 as a function of gate voltage V_g and source-drain voltage bias V_{sd} . **b**, Vertical cuts in **a** in the tunneling (red line) and one-channel (blue line) regime. **c**, Differential conductance at zero source-drain voltage, $G(V_{\text{sd}} = 0 \text{ mV})$, versus averaged differential conductance at finite source-drain voltage, $G(|V_{\text{sd}}| > 0.8 \text{ mV})$. Red and blue circles indicate data corresponding to cuts in **b**. Green line is theoretical prediction for conductance in an Andreev enhanced QPC (Eq. (1) with no fitting parameters).

mixing when a new channel opens, leading to a reduction in transparency of the already open first channel. A constant contact resistance $R_c \sim 1 \text{ k}\Omega$ has been subtracted in each viewgraph, a value chosen to move the first plateau in the normal state to G_0 .

By further depleting the electron gas in the constriction, the device is operated as a tunnel probe of the local density of states in the InAs 2DEG. This technique has been applied to studying subgap properties of semiconductor nanowires coupled to superconductors [15–17, 19, 29, 30]. In Fig. 3a the QPC voltage is decreased to gradually transition from the one-channel regime, where the zero bias conductance is $4e^2/h$, to the tunneling regime, where conductance is strongly suppressed for $|V_{sd}| < 190 \text{ }\mu\text{V}$. From these measurements, the gap in the density of states of the InAs due to the proximity to the Al is estimated to be $\Delta^* \sim 190 \text{ }\mu\text{eV}$ (measured peak-to-peak). The value of Δ^* is similar, but not identical, to the gap in the Al film as estimated from T_c , as discussed above.

In the case of perfect Andreev reflection from the superconductor/semiconductor interface, the conductance of one channel through a constriction proximal to the interface is given by

$$G_{ns} = 2G_0 \frac{G_{nn}^2}{(2G_0 - G_{nn})^2}, \quad (1)$$

where G_{ns} is the conductance when the film is superconducting, and G_{nn} is the conductance in the normal state [14]. In Fig. 3c the prediction in Eq. (1) with no free parameters (green line) and experimental data are shown. Here, G_{nn} is the average conductance for $|V_{sd}| > 0.8 \text{ mV}$, justified by the equality of applying a bias and raising the temperature above T_c , as shown in Fig. 2a. Equation (1) is consistent with the data over two orders of magnitude in G_{ns} , indicating that the zero bias conductance up to $4e^2/h$ is well described by the prediction of perfect Andreev reflection of a single QPC mode. However, the systematic deviation between data and prediction in Fig. 3c for $G_{ns} < 10^{-2} 2e^2/h$ could be a manifestation of a small remnant non-zero normal scattering probability.

The shapes of the conductance curves at $eV_{sd} \lesssim \Delta^*$ in the tunneling regime (red line in Fig. 3b) are smeared relative to the conventional Bardeen-Cooper-Schrieffer (BCS) density of states of a superconductor. This could be due to broadening of the BCS coherence peaks in the disordered superconducting film formed in the 2DEG under the Al [31], a weak coupling between Al and 2DEG [18] or the layout of the tunnel probe relative to the proximitized 2DEG [32–34].

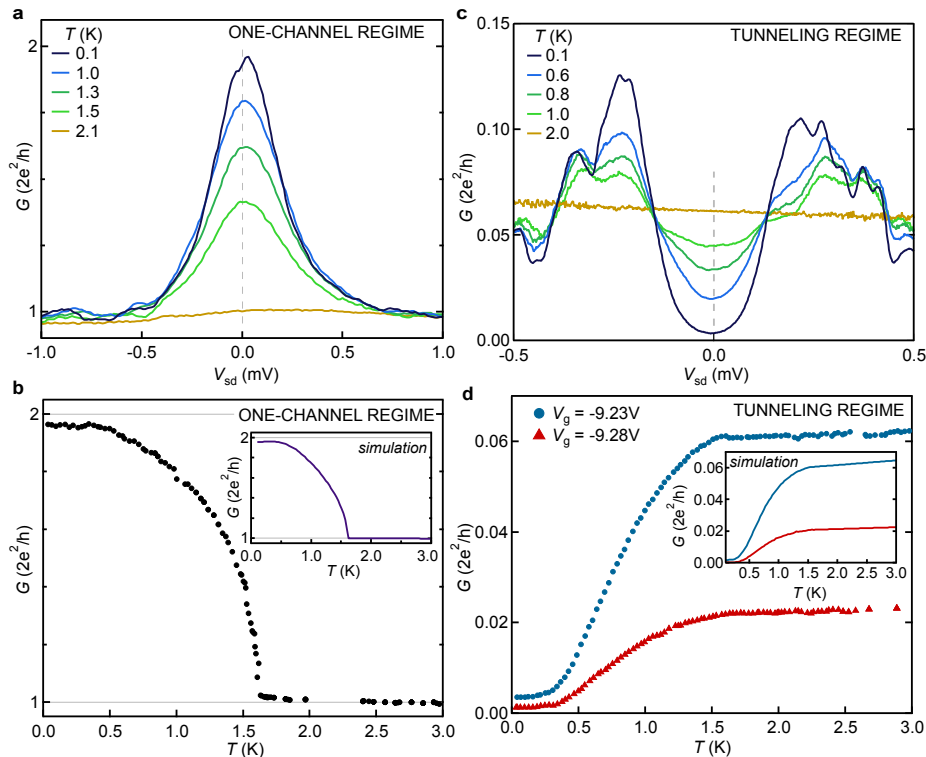


FIG. 4: **Temperature dependence of the enhanced subgap conductance and the hard superconducting gap.** **a**, Differential conductance, G , as a function of source-drain bias voltage, V_{sd} , at five temperatures in the one-channel regime. **b**, Temperature dependence at zero bias (dashed, gray line in **a**) in the one-channel regime. **c**, Similar measurement to **a**, but in the tunneling regime. **d**, As in **b**, for two different values of gate voltage, V_g , both in the tunneling regime. Insets in **b** and **d** show results from numerical simulations (see main text and supplement for details).

The temperature dependence of the conductance in the Andreev QPC is different in the one-channel and in the tunnel regime (Fig. 4). The one-channel regime (Fig. 4a,b) has a pronounced kink at $T = T_c$, presumably associated with the sudden onset of Andreev enhanced subgap conductance. In contrast, the temperature-dependence in the tunnel regime (Fig. 4c,d) is smeared close to T_c due to thermally excited quasiparticles.

The temperature dependence is simulated (insets in Fig. 4) by calculating $G = \int dE \mathcal{G}(E) (-\frac{\partial f}{\partial E})$ where f is the Fermi function which accounts for thermal broadening. The conductance $\mathcal{G}(E)$ is calculated by combining scattering matrices of quasielectrons and quasiholes in the normal region and Andreev reflection at the superconductor interface (details given in supplementary materials). The scattering matrices are calculated using the numerical package Kwant [35], and the simulation is performed using the device geometry from the micrograph in Fig. 1b. The temperature dependence of the gap is modeled with $\Delta^*(T) = \Delta^* \sqrt{1 - (T/T_c)^2}$, and the Andreev reflection amplitude is taken from [14]. The simulation shows good quantitative agreement with the data.

To drive a superconductor/semiconductor device into a topological regime, one requirement is $g\mu_B B > \Delta^*$, while the native superconductor retains its gap. Figure 5 shows the in-plane magnetic field dependence of Δ^* , from which an approximate critical field $B_c^* \sim 300$ mT is extracted. A rough estimate of the g -factor can be inferred by assuming the critical B_c^* results from Zeeman energy surpassing the induced superconducting gap, that is $g\mu_B B_c^* = \Delta^*$, which yields $g \sim 10$, similar to the g -factor in bulk InAs. In Fig. 5d the zero-bias conductance is shown for the two different in-plane directions, and the slight direction dependence of B_c^* could be due to an anisotropic g -factor in the InAs crystal lattice. The induced gap in the 2DEG disappears at in plane magnetic fields significantly smaller than the critical field of the Al film itself. Taken together with the strong spin-orbit interaction ($l_{so} \sim 45$ nm), allows this superconductor-2DEG system to be driven into the topological regime, where the Zeeman energy should close the gap in the semiconductor, while the parent superconductor retains its superconducting properties.

In conclusion, we observe quantization doubling through a QPC proximal to a superconductor/semiconductor interface, confirming a long-standing theoretical prediction [14]. Operated as a gate-tunable tunnel probe of the local density of states, the QPC shows a hard superconducting gap induced in the 2DEG. The magnetic field dependence of the induced gap compares favorably with the critical field of the superconducting film, opening possibilities to pursue topological states of matter in one-dimensional structures fabricated from epitaxial Al/2D InAs material.

Acknowledgements: Research support by Microsoft Project Q, the Danish National Research Foundation.

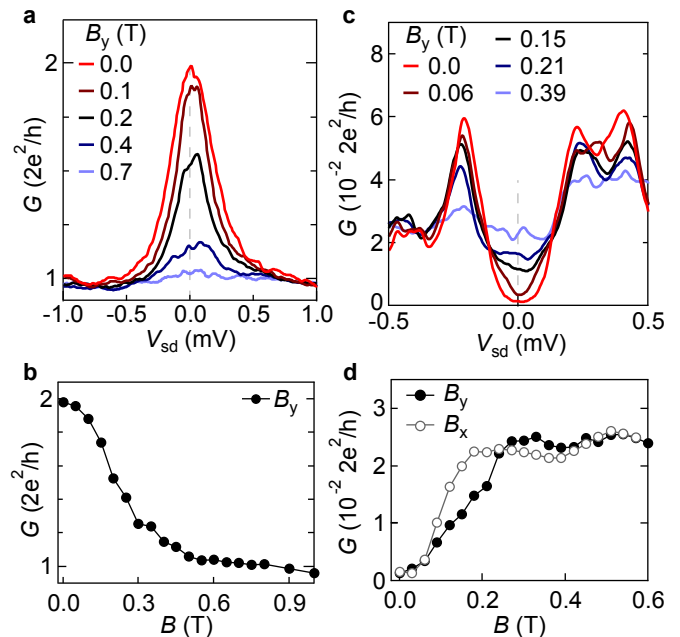


FIG. 5: **In plane magnetic field of the enhanced subgap conductance and the hard superconducting gap.** **a**, Differential conductance, G , as a function of source-drain bias, V_{sd} , at several in-plane magnetic fields applied along the point contact constriction. **b**, Zero-bias conductance as a function of the in-plane magnetic field, B_y . **c**, Similar measurement to **a** but in the tunneling regime. **d**, As in **b**, but in the tunneling regime, for both in-plane directions (B_y is along and B_x is perpendicular to the constriction).

C.M.M. acknowledges support from the Villum Foundation. F.N. acknowledges support from a Marie Curie Fellowship (No. 659653). M.P.N. acknowledges support from ERC Synergy Grant. A.A. is supported by an ERC Starting Grant. M.W. and A.A. are supported by the Foundation for Fundamental Research on Matter (FOM) and the Netherlands Organization for Scientific Research (NWO/OCW) as part of the Frontiers of Nanoscience program. We are indebted to S. Kraemer for the TEM analysis, performed at the UCSB MRL Shared Experimental Facilities (NSF DMR 1121053), a member of the NSF-funded Materials Research Facilities Network.

-
- * Now at City College, City University of New York
- [1] Takayanagi, H., Hansen, J. B. & Nitta, J. Mesoscopic Fluctuations of the Critical Current in a Superconductor—Normal-Conductor—Superconductor. *Physical Review Letters* **74**, 166–169 (1995).
 - [2] Rahman, F. *et al.* Superconductor-semiconductor interaction effects in mesoscopic hybrid structures. *Physical Review B* **54**, 14026–14031 (1996).
 - [3] Fazio, R. Quantum phase transitions and vortex dynamics in superconducting networks. *Physics Reports* **355**, 235–334 (2001).

- [4] Chrestin, A., Matsuyama, T. & Merkt, U. Critical currents and supercurrent oscillations in Josephson field-effect transistors. *Physical Review B* **49**, 498–504 (1994).
- [5] Akazaki, T., Takayanagi, H., Nitta, J. & Enoki, T. A Josephson field effect transistor using an InAs-inserted-channel $\text{In}_{0.52}\text{Al}_{0.48}\text{As}/\text{In}_{0.53}\text{Ga}_{0.47}\text{As}$ inverted modulation-doped structure. *Applied Physics Letters* **68**, 418–420 (1996).
- [6] Alicea, J. Majorana fermions in a tunable semiconductor device. *Physical Review B* **81**, 125318 (2010).
- [7] Lutchyn, R. M., Sau, J. D. & Das Sarma, S. Majorana Fermions and a Topological Phase Transition in Semiconductor-Superconductor Heterostructures. *Physical Review Letters* **105**, 077001 (2010).
- [8] Oreg, Y., Refael, G. & von Oppen, F. Helical Liquids and Majorana Bound States in Quantum Wires. *Physical Review Letters* **105**, 177002 (2010).
- [9] Takayanagi, H. & Akazaki, T. Andreev Reflection at the Superconductor-2-Dimensional-Electron-Gas Interface by a Quantum Point-Contact. *Physical Review B* **52**, R8633–R8636 (1995).
- [10] Amado, M. *et al.* Electrostatic tailoring of magnetic interference in quantum point contact ballistic Josephson junctions. *Physical Review B* **87**, 134506 (2013).
- [11] Irie, H., Harada, Y., Sugiyama, H. & Akazaki, T. Josephson coupling through one-dimensional ballistic channel in semiconductor-superconductor hybrid quantum point contacts. *Physical Review B* **89**, 165415 (2014).
- [12] Shabani, J. *et al.* Two-dimensional epitaxial superconductor-semiconductor heterostructures: A platform for topological superconducting networks. *submitted for publication. Preprint available at arXiv/1511.01127*.
- [13] Takei, S., Fregoso, B. M., Hui, H.-Y., Lobos, A. M. & Das Sarma, S. Soft Superconducting Gap in Semiconductor Majorana Nanowires. *Physical Review Letters* **110**, 186803 (2013).
- [14] Beenakker, C. W. J. Quantum transport in semiconductor-superconductor microjunctions. *Physical Review B* **46**, 12841–12844 (1992).
- [15] Mourik, V. *et al.* Signatures of Majorana Fermions in Hybrid Superconductor-Semiconductor Nanowire Devices. *Science* **336**, 1003–1007 (2012).
- [16] Das, A. *et al.* Zero-bias peaks and splitting in an Al-InAs nanowire topological superconductor as a signature of Majorana fermions. *Nature Physics* **8**, 887–895 (2012).
- [17] Deng, M. T. *et al.* Anomalous Zero-Bias Conductance Peak in a Nb–InSb Nanowire–Nb Hybrid Device. *Nano Letters* **12**, 6414–6419 (2012).
- [18] Cole, W. S., Das Sarma, S. & Stanescu, T. D. Effects of large induced superconducting gap on semiconductor Majorana nanowires. *Physical Review B* **92**, 174511 (2015).
- [19] Chang, W. *et al.* Hard gap in epitaxial semiconductor-superconductor nanowires. *Nature Nanotechnology* **10**, 232–236 (2015).
- [20] Higginbotham, A. P. *et al.* Parity lifetime of bound states in a proximitized semiconductor nanowire. *Nature Physics* **11**, 1017–1021 (2015).
- [21] Takayanagi, H., Akazaki, T. & Nitta, J. Observation of Maximum Supercurrent Quantization in a Superconducting Quantum Point-Contact. *Physical Review Letters* **75**, 3533–3536 (1995).
- [22] Bauch, T. *et al.* Correlated quantization of supercurrent and conductance in a superconducting quantum point contact. *Physical Review B* **71**, 174502 (2005).
- [23] Jakob, M. *et al.* Direct determination of the Andreev reflection probability by means of point contact spectroscopy. *Applied Physics Letters* **76**, 1152–1154 (2000).
- [24] Deon, F. *et al.* Quantum dot spectroscopy of proximity-induced superconductivity in a two-dimensional electron gas. *Applied Physics Letters* **98**, 132101 (2011).
- [25] Deon, F. *et al.* Proximity effect in a two-dimensional electron gas probed with a lateral quantum dot. *Physical Review B* **84**, 100506 (2011).
- [26] Andreev, A. F. The Thermal Conductivity of the Intermediate State in Superconductors. *Soviet Physics JETP-Ussr* **19**, 1228–1231 (1964).
- [27] Chubov, P. N., Eremenko, V. V. & Pilipenko, Y. A. Dependence of the critical temperature and energy gap on the thickness of superconducting aluminum films. *JETP Letters* **28** (1969).
- [28] Mortensen, N. A., Jauho, A.-P., Flensberg, K. & Schomerus, H. Conductance enhancement in quantum-point-contact semiconductor-superconductor devices. *Physical Review B* **60**, 13762–13769 (1999).
- [29] Churchill, H. O. H. *et al.* Superconductor-nanowire devices from tunneling to the multichannel regime: Zero-bias oscillations and magnetoconductance crossover. *Physical Review B* **87**, 241401 (2013).
- [30] Lee, E. J. H. *et al.* Spin-resolved Andreev levels and parity crossings in hybrid superconductor-semiconductor nanostructures. *Nature Nanotechnology* **9**, 79–84 (2014).
- [31] Feigel'man, M. V. & Skvortsov, M. A. Universal Broadening of the Bardeen-Cooper-Schrieffer Coherence Peak of Disordered Superconducting Films. *Physical Review Letters* **109**, 147002 (2012).
- [32] Guéron, S., Pothier, H., Birge, N. O., Esteve, D. & Devoret, M. H. Superconducting Proximity Effect Probed on a Mesoscopic Length Scale. *Physical Review Letters* **77**, 3025–3028 (1996).
- [33] le Sueur, H., Joyez, P., Pothier, H., Urbina, C. & Esteve, D. Phase Controlled Superconducting Proximity Effect Probed by Tunneling Spectroscopy. *Physical Review Letters* **100**, 197002 (2008).
- [34] Cherkez, V. *et al.* Proximity Effect between Two Superconductors Spatially Resolved by Scanning Tunneling Spectroscopy. *Physical Review X* **4**, 011033 (2014).
- [35] Groth, C. W., Wimmer, M., Akhmerov, A. R. & Waintal, X. Kwant: a software package for quantum transport. *New Journal of Physics* **16**, 063065 (2014).

Supplementary material: Quantized conductance doubling and hard gap in a two-dimensional semiconductor-superconductor heterostructure

FINITE BIAS MEASUREMENTS OF THE TRANSITION FROM $4e^2/h$ TO HARD GAP

The data in Fig. 3 of the main text is measured in a DC setup, incrementing the voltage in steps of size $3 \mu\text{V}$. The data is smoothed over 10 steps and the derivative is calculated numerically to obtain the differential conductance. A constant contact resistance $R_c = 800 \Omega$ is subtracted from the data, moving the conductance at $V_g = -8.2 \text{ V}$ for $V_{sd} > 0.8 \text{ mV}$ to $2e^2/h$. The 4-terminal resistance of the device is $R_d = 400 \Omega$ with $V_g = 0 \text{ V}$. The difference between R_c and R_d is most likely dominated by the change of resistivity near the gated region, when the gate is turned on, as well as the distance from the voltage probe to the QPC region. The voltage probes are located $\sim 15 \mu\text{m}$ away from the QPC and the gates overlap the mesa over an area $\sim 1.6 \mu\text{m}^2$. The normal state conductance is calculated as the average of $G(V_{sd})$ for V_{sd} in the range $[\pm 0.8 \text{ mV}, \pm 1 \text{ mV}]$. The analysis is largely unaffected by changing the averaging window for values $|V_{sd}| > 0.6 \text{ mV}$. The cuts in Fig. 3b are taken by averaging over a 12 mV (30 mV) window in V_g for the one-channel (tunneling) regime. Finally, each datapoint in Fig. 3c is calculated as the average over a 10 mV range in V_g .

MEASUREMENTS ON ALTERNATE WAFER

Under identical growth conditions, a wafer without an InGaAs top barrier (i.e. $b = 0 \text{ nm}$) between the epitaxial aluminum and the InAs quantum well was produced. The density and mobility, measured using a conventional Hall bar geometry, was $n = 4.5 \cdot 10^{16} \text{ m}^{-2}$ and $\mu = 4000 \text{ cm}^2/\text{Vs}$, corresponding to a mean free path of $l_e = 150 \text{ nm}$. In a lithographically similar device to that shown in Fig. 1 of the main text, we observe a hard superconducting gap (Fig. S1). When the gates are operated in the quantum point contact regime, we did not observe quantized steps in conductance. The non-monotonic decrease in conductance at $V_{sd} = 0 \text{ mV}$, believed to be due to disorder in the 2DEG, makes the identification of a superconducting gap in this wafer difficult (Fig. S1b).

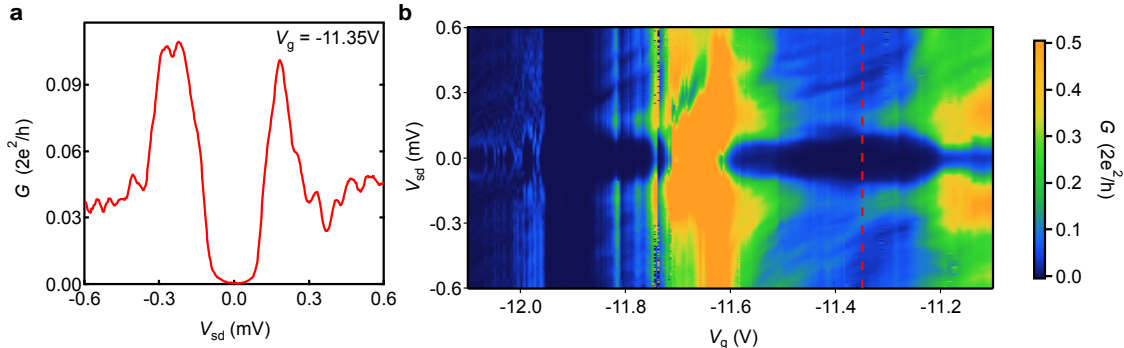


FIG. S1: **Spectroscopy of the superconducting gap in a wafer with 0 nm InGaAs barrier.** **a**, Differential conductance, G , as a function of source-drain voltage, V_{sd} , in a quantum point contact geometry, with gate voltage $V_g = -11.35 \text{ V}$. **b**, Differential conductance at finite source-drain voltage, as the split-gate is used to deplete the 2DEG by decreasing V_g . Vertical cut in **a** indicated by dashed, red line.

However, by increasing the temperature (Fig. S2a) or the magnetic field (Fig. S2b) we confirm that the gap in the density of states in Fig. S1 is related to the superconducting properties of the aluminum film.

Model for numerical simulations

We calculate the conductance of the junction in two steps. Firstly, we determine the scattering properties of the normal region which we assume is a $1.1 \mu\text{m}$ wide channel of length L , where we have taken dimensions from SEM in Fig. 1b in the main text. It is described by the spinless Hamiltonian,

$$H = \frac{\hbar^2 \mathbf{k}^2}{2m^*} + V_{QPC}(x, y) + V_d(x, y) - \mu. \quad (\text{S1})$$

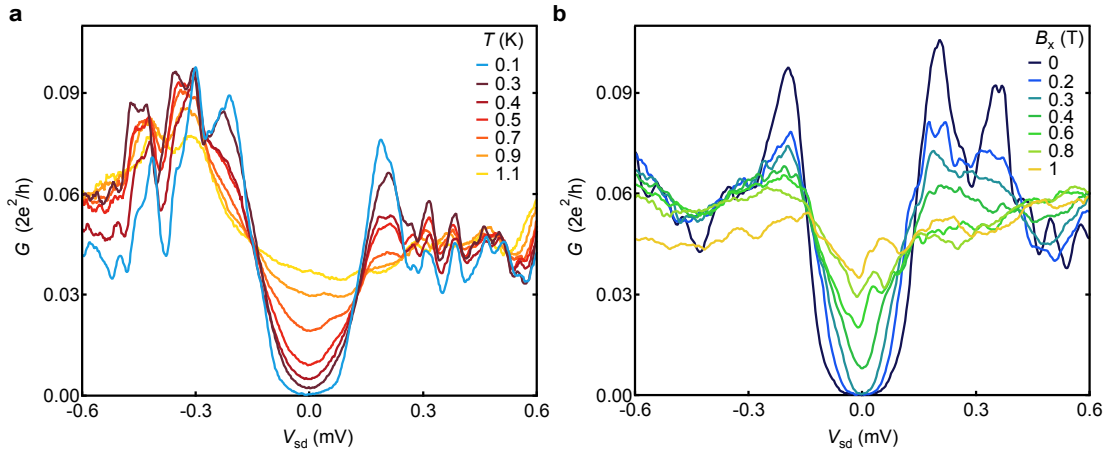


FIG. S2: **Temperature and magnetic field dependence of the proximity induced superconducting gap.** a, Differential conductance as a function of source-drain voltage for several temperatures. b, In-plane magnetic field dependence of the superconducting gap (field applied perpendicular to the constriction).

We model the QPC as two rectangular gates located at $x = 400$ nm, with the width $2W$, separated by the length $2S$ and located at the distance d above 2DEG (see Fig. S3). We calculate the potential generated by the QPC electrodes $V(x, y)$ for the gate voltage V_g following [S1], with

$$\frac{V_{QPC}(x, y)}{-eV_g} = \frac{1}{\pi} \left[\arctan\left(\frac{W+x}{d}\right) + \arctan\left(\frac{W-x}{d}\right) \right] - g(S+y, W+x) - g(S+y, W-x) - g(S-y, W+x) - g(S-y, W-x), \quad (\text{S2})$$

where

$$g(u, v) = \frac{1}{2\pi} \arctan\left(\frac{uv}{dR}\right), \quad (\text{S3})$$

and $R = \sqrt{u^2 + v^2 + d^2}$. We include disorder [S2] by adding a random on-site energy $V_d(x, y)$ distributed uniformly

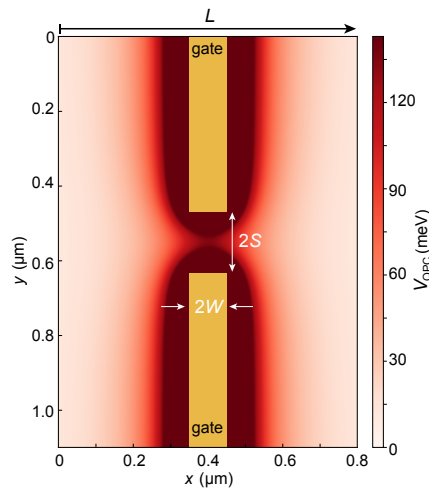


FIG. S3: **QPC potential layout.** The yellow contours show the geometry of the QPC gates and the red color depicts potential created at the position of 2DEG for $V_g = -1350$ mV.

between $-W/2$ and $W/2$ where

$$W = \mu \sqrt{\frac{6\lambda_F^3}{\pi^3 \Delta x^2 l_e}}. \quad (\text{S4})$$

Due to limitation of the computational mesh resolution we exclude the disorder from the vicinity of the QPC and take $W \neq 0$ only for $x > 700$ nm.

We calculate the scattering matrix of the normal part of the junction for a quasiparticle at the energy ε as

$$S_N(\varepsilon) = \begin{pmatrix} r(\varepsilon) & t(\varepsilon) \\ t'(\varepsilon) & r'(\varepsilon) \end{pmatrix}, \quad (\text{S5})$$

using Kwant package [S3] and discretizing the Hamiltonian in Eq. (S1) on a mesh with the spacing $\Delta x = \Delta y = 3$ nm. The quantities $r(E)$ and $t(E)$ denote reflection and transmission submatrices for a time-reversal symmetric system.

In the second step, we combine the scattering matrices calculated for ε and $-\varepsilon$ (that correspond to quasidelectron and quasihole respectively) with the matrix that accounts for the Andreev reflection at the superconductor interface

$$S_A = r_A \begin{pmatrix} 0 & e^{i\phi} \\ e^{-i\phi} & 0 \end{pmatrix}, \quad (\text{S6})$$

where

$$r_A = \frac{\varepsilon}{\Delta(T)} - i \operatorname{sign}[\varepsilon + \Delta(T)] \sqrt{1 - \frac{\varepsilon^2}{\Delta(T)^2}}. \quad (\text{S7})$$

The latter equation describes the Andreev reflection amplitude [S4] including the temperature dependent pairing potential $\Delta(T) = \Delta^* \sqrt{1 - (T/T_c)^2}$. Finally we calculate the conductance according to

$$G_{ns}(E) = \int d\varepsilon \mathcal{G}(\varepsilon) \left(-\frac{\partial f(E, \varepsilon)}{\partial \varepsilon} \right), \quad (\text{S8})$$

where f stands for the Fermi function

$$f(E, \varepsilon) = \frac{1}{e^{(\varepsilon - E)/k_b T} + 1}, \quad (\text{S9})$$

and where $\mathcal{G}(\varepsilon) = N - \|r_e(\varepsilon)\|^2 + \|r_h(\varepsilon)\|^2$. N is the number of modes in the normal lead. The quasidelectron and quasihole reflection matrices are given by:

$$r_e(\varepsilon) = r(\varepsilon) + t'(\varepsilon) r_A r'^*(-\varepsilon) r_A \frac{1}{1 - r'(\varepsilon) r_A r'^*(-\varepsilon) r_A} t(\varepsilon), \quad (\text{S10})$$

$$r_h(\varepsilon) = t'^*(-\varepsilon) r_A \frac{1}{1 - r'(\varepsilon) r_A r'^*(-\varepsilon) r_A} t(\varepsilon). \quad (\text{S11})$$

Additionally, the normal-state conductance is given by $G_{nn} = \|t(\varepsilon = 0)\|^2$.

Numerical results

For the simulation we adopt the following parameters: chemical potential $\mu = 143$ meV, mean free path $l_e = 230$ nm, effective mass $m^* = 0.05m_e$ (obtained from $k.p$ calculation of the Fermi velocity for a single mode quantum well in the growth direction). We also assume $T_c = 1.6$ K and $\Delta^* = 190$ μ eV. The QPC geometry is set by the parameters: $W = 50$ nm (width of gates), $S = 75$ nm (separation between gates) and $d = 50$ nm (distance from gates down to the 2DEG).

We consider a system of the geometry similar to the one presented on Fig. 1b of the main text. Here the superconductor interface is located 230 nm after the QPC.

Figure S4a shows the conductance as a function of the gate voltage. The G_{ns} conductance depicted with the black curve is quantized in multiples of $4e^2/h$ as the transport involves transmission of an electron and an Andreev-reflected hole. Figures S4b,c show the Andreev-enhanced spectroscopy curves obtained by varying the injection energy E . Figure S4b and S4c show, respectively, the calculated finite-bias properties of the one-channel regime and the tunneling regime, for several values of the temperature. The value of V_g in the simulations are chosen so the conductance at zero bias match the data at $T > T_c$ in Fig. 4 of the main text. The low temperature spectroscopy

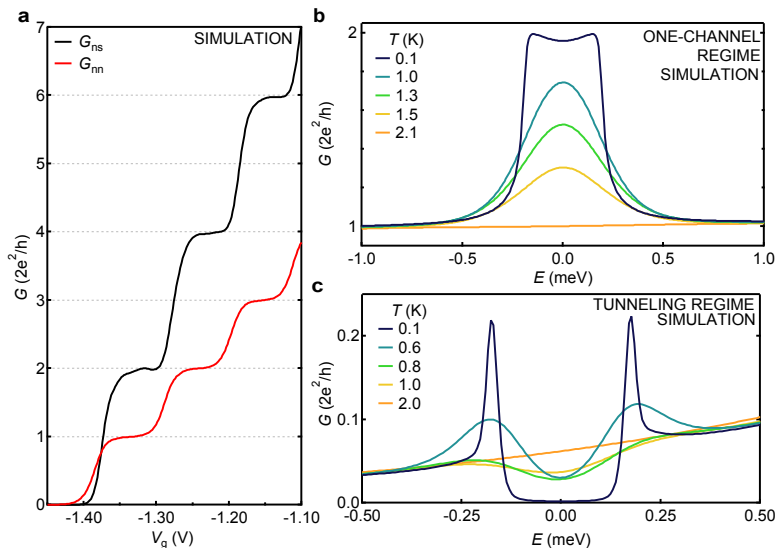


FIG. S4: **Conductance calculated for a system with $L = 680$ nm.** **a** Andreev-enhanced conductance G_{ns} (black curve) and the normal-state conductance G_{nn} (red curve) versus the potential on the QPC gates calculated for $E = 0$. **b** Spectroscopy curves in one-channel regime for $V_g = -1330$ mV. **c** Tunneling spectroscopy curves for $V_g = -1408.7$ mV.

curves are similar the ones obtained by using the analytic expression of Blonder-Tinkham-Klapwijk (BTK) [S5]. However, for energies larger than the gap, the spectroscopy simulations show an increasing trend as a function of E (cf. the orange curves on Fig. S4b,c where $T > T_c$), due to an increase of the energy of the injected particle with respect to the QPC potential. This dependence is pronounced in our geometry, because the slopes of the QPC steps are less than 50 meV wide, making the conductance sensitive to changes in E on the scale of single meV.

The low temperature one-channel spectroscopy curve shows maxima at $|E| \simeq \Delta$ (blue curve in Fig. S4b) while in the experimental data (cf. Fig. 4a and Fig. 5a of the main text) the curves decrease smoothly as $|V_{sd}|$ is increased. Previous theoretical work [S6] showed that the detailed layout of the interface between the normal and superconducting electrodes (at the scale of the coherence length) impacts the subgap conductance due to interference between two electrons tunneling through the interface. Moreover, smearing of the superconducting coherence peak [S7] is predicted to be an effect of disorder present in the superconducting film pointing again to the role of normal-superconductor interface.

The experimental structure consist of an extended 2DEG/superconductor interface created by the InGaAs/InAs heterostructure covered by Al. In the present calculations, we are limited to an abrupt semiconductor/superconductor interface. We therefore also consider a case where the distance from the QPC to the interface is increased relative to the lithographic dimensions.

Figure S5 shows results obtained for a system with 800 nm distance between the QPC gates and the superconductor interface. In this calculation the scattering region is longer than the mean free path, leading to the peak/dip structures superimposed on the QPC conductance steps. Similar peaks/dips are observed in the experimental data in Figs. 2a,b of the main text. The fluctuations are more pronounced in the superconducting case (G_{ns}) due to the Andreev-enhanced conductance involving traversing the scattering region twice. The resonant features are also visible in the low temperature spectroscopy curves for energies larger the superconducting gap (cf. Figs. S5b,c), similar to the experimental curves in Figs. 4 a,c. Comparable pinch off curves are obtained when the disorder is located before the QPC, if the distance between the QPC and the superconductor are short.

The most notable feature of the system with extended length between the QPC and the superconductor is a significant reduction of the width of the central peak in the one-channel finite-bias simulations (blue curve in Fig. S5b). The rapid drop in conductance is a hallmark of an induced gap, for which the chaotic billiard in the region between the QPC gates and superconductor has zero density of states. The energy scale at which conductance drops is denoted E_b , and has the magnitude of Thouless energy [S8, S9], and hence it is inversely proportional to the area between the QPC and the interface. For $|E| > E_b$ the billiard has a non-zero discrete spectrum and so for $E_b < |E| < \Delta$ the conductance exhibits oscillations due to transport through resonant states which here are smoothed already for $T = 0.1$ K due to temperature averaging. The smooth resonances are also present in the low-temperature conductance curve in the tunneling regime (Fig. S5c).

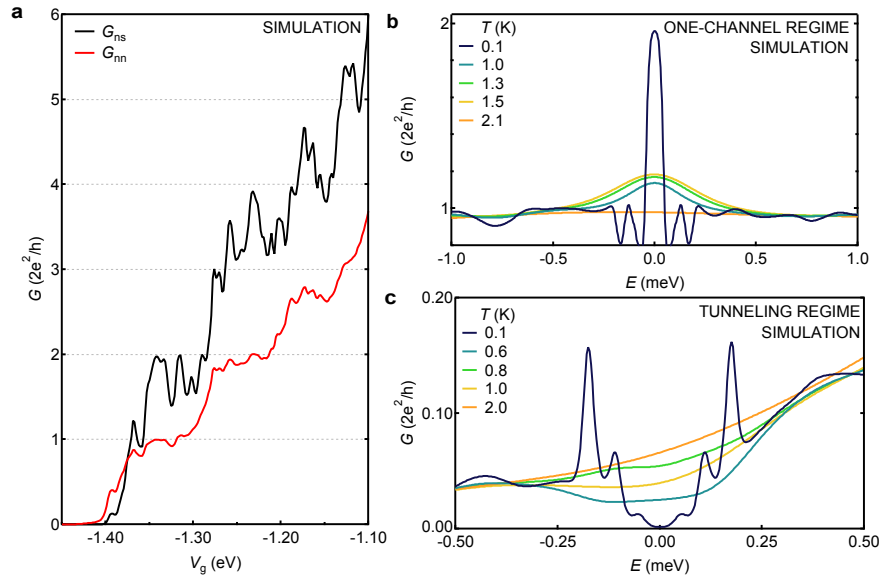


FIG. S5: **Conductance calculated for a system with $L = 1250$ nm.** **a** Andreev-enhanced conductance G_{ns} (black curve) and the normal-state conductance G_{nn} (red curve) versus the potential on the QPC gates calculated for $E = 0$. **b** Spectroscopy curves in the one-channel regime for $V_g = -1341$ mV. **c** Tunneling spectroscopy curves for $V_g = -1407$ mV.

* Now at City College, City University of New York

- [S1] Davies, J. H., Larkin, I. A. & Sukhorukov, E. V. Modeling the patterned twodimensional electron gas: Electrostatics. *Journal of Applied Physics* **77**, 4504–4512 (1995).
- [S2] Ando, T. Quantum point contacts in magnetic fields. *Phys. Rev. B* **44**, 8017–8027 (1991).
- [S3] Groth, C. W., Wimmer, M., Akhmerov, A. R. & Waintal, X. Kwant: a software package for quantum transport. *New J. Phys.* **16**, 063065 (2014).
- [S4] Beenakker, C. W. J. Quantum transport in semiconductor-superconductor microjunctions. *Phys. Rev. B* **46**, 12841–12844 (1992).
- [S5] Blonder, G. E., Tinkham, M. & Klapwijk, T. M. Transition from metallic to tunneling regimes in superconducting microconstrictions: Excess current, charge imbalance, and supercurrent conversion. *Phys. Rev. B* **25**, 4515–4532 (1982).
- [S6] Hekking, F. W. J. & Nazarov, Y. V. Subgap conductivity of a superconductor-normal-metal tunnel interface. *Phys. Rev. B* **49**, 6847–6852 (1994).
- [S7] Feigelman, M. V. & Skvortsov, M. A. Universal Broadening of the Bardeen-Cooper-Schrieffer Coherence Peak of Disordered Superconducting Films. *Phys. Rev. Lett.* **109**, 147002 (2012).
- [S8] Melsen, J. A., Brouwer, P. W., Frahm, K. M. & Beenakker, C. W. J. Induced superconductivity distinguishes chaotic from integrable billiards. *Europhysics Letters (EPL)* **35**, 7–12 (1996).
- [S9] Melsen, J. A., Brouwer, P. W., Frahm, K. M. & Beenakker, C. W. J. Superconductor-proximity effect in chaotic and integrable billiards. *Phys. Scr.* **1997**, 223 (1997).